3D PET-DRIVEN MULTI-PHASE SEGMENTATION OF MENINGIOMAS IN MRI

H. Urien[⋆†] *I. Buvat*[⋆] *N. Rougon*[†] *S. Boughdad*[†⋆] *I. Bloch*[⋆†]

[⋆†] LTCI, CNRS, Télécom ParisTech, Université Paris-Saclay, 75013, Paris, France
[⋆] IMIV, Inserm, CEA, Université Paris-Sud, CNRS, Université Paris-Saclay, 91400, Orsay
[†⋆] Institut Curie, Hôpital René Huguenin, Département d'Imagerie médicale,
35 rue Dailly, 92210 Saint-Cloud, France
[†] MAP5, CNRS, Télécom SudParis, Université Paris-Saclay, 91011, Evry, France

ABSTRACT

Combining anatomical and functional information from Magnetic Resonance Imaging (MRI) and Positron Emission Tomography (PET) scans brings great opportunities to improve diagnosis in oncology and treatment planning in radiation oncology. In this work, we propose a PET-guided MR tumor segmentation method minimizing a globally convex energy in a multiphase framework to account for the context variability of lesions. The method was evaluated in four patients with atypical meningiomas of different shapes, locations and metabolism, and the Dice index obtained by comparing with a manual tumor segmentation performed by an expert was 0.65 ± 0.13. The results demonstrated a good ability of the method to differentiate tumors from tissues with similar MRI intensity values.

Index Terms— Multimodal segmentation, variational method, Brain Tumor, Positron Emission Tomography (PET), Magnetic Resonance Imaging (MRI)

1. INTRODUCTION

Multimodality imaging in oncology is used to improve diagnosis and treatment planning by making the most of the complementary properties of each image involved. For example, PET reveals suspicious areas of high tracer uptake, and so highlights potential tumor activity, while the high resolution of MRI allows confirming tumor location and delineating precisely pathological structures. This paper aims at using PET metabolic information to improve the delineation of brain tumors in MR images.

Combining PET and MRI raises new challenges. Multimodality imaging must cope with the different resolution and intensity properties of the two modalities. In addition, the MR signal suffers from a great variability, and is not normalized against a standard scale unlike the Hounsfield scale used in Computed Tomography (CT).

Several multimodal segmentation methods have addressed the joint use of anatomical and functional information, especially in PET-CT. Most of them lead to a single tumor volume [1, 2], which does not account for the specific nature of boundaries in each modality, and can be biased by registration issues. The only method delineating two specific tumor volumes in PET-CT [3] requires many parameters to be set, while other promising models segmenting anatomical modalities using PET information have emerged [4, 5].

In this paper, we propose a new PET-driven MR segmentation, extending the method from [5] to a multi-phase framework to capture the variability of the tumor surroundings. Starting from the unimodal two-phase segmentation model, we first present its four-phase extension before detailing the mechanism for integrating PET information. The resulting multimodal four-phase segmentation method is evaluated both quantitatively and qualitatively and then discussed.

2. A 3D MULTI-PHASE PET-DRIVEN MRI SEGMENTATION METHOD

Image segmentation aims at finding a partition of an image into several regions (or phases). This can be performed using a variational approach where the optimal segmentation minimizes an energy criterion depending on region and boundary features. Popular methods emerged, such as the one by Chan [6] who changed the two-phase level set method based on the piecewise-constant Mumford-Shah model [7] into a convex formulation insensitive to local minima.

In this paper, a four-phase model is used to account for the potentially heterogeneous signal around the tumor: one phase is assigned to the tumor and three to the surrounding tissues.

2.1. 3D multi-phase unimodal segmentation

In [8], a four-phase piecewise constant formulation of the segmentation problem was derived for a single modality, based on the two-phase model from [6]. This four-phase extension allows jointly modeling the tumor and its surroundings while keeping an initialization-independent model. It is built by combining two two-phase models, respectively defined by the membership functions $u = (u_1, u_2) \in [0,1]^2$. We propose a compact formulation using phase mixing functions $\varphi_{ij}(t,t') = \varphi_i(t)\varphi_j(t')$ where $\varphi_i : [0,1] \longrightarrow [0,1]$, $i \in \{0,1\}$ is defined as:

$$\varphi_i(t) = \begin{cases} t & \text{if } i = 1 \\ 1-t & \text{if } i = 0 \end{cases}$$

Starting from an initial partition of the MR image domain Ω, the segmentation problem is solved by minimizing an energy E [8]:

$$E(u,c) = \int_\Omega \mu_1 \left|\nabla u_1(x)\right| dx + \int_\Omega \mu_2 \left|\nabla u_2(x)\right| dx + \sum_{(i,j)\in\{0,1\}^2} \int_\Omega \lambda_{ij}\varphi_{ij}(u_1(x),u_2(x))(I_{\mathrm{MRI}}(x) - c_{ij})^2 dx \quad (1)$$

where $I_{\mathrm{MRI}}(x)$ is the normalized MRI intensity of voxel x, μ_1, μ_2, λ_{ij}, $(i,j) \in \{0,1\}^2$ are positive hyperparameters and $c = (c_{11}, c_{01}, c_{10}, c_{00})$ are the constant approximations of the MRI intensity in the various phases. Normalization of the MRI intensity addresses the MR signal variability associated with the tumor type or device.

978-1-4799-2349-6/16/$31.00 ©2016 IEEE

This energy is composed of two parts. On the one hand, the regularization terms, weighted by the μ_i constants, enforce a minimal-length constraint on the boundary of each phase, which ensures the smoothness of the segmentation (the gradient operator characterizes the contours). On the other hand, the data consistency terms, weighted by the λ_{ij} constants, ensure that the voxels belonging to the same phase share common features, here the same MRI intensity (hence the term of "piecewise constant" formulation). Moreover, the membership of a voxel to a phase is embedded in the φ_{ij} functions and depends jointly on u_1 and u_2. Thus, the six hyperparameters control the trade-off between smoothness prior and region homogeneity.

This model is called "fuzzy" because the segmentation functions u_1 and u_2 have values in $[0, 1]$ rather than in $\{0, 1\}$ as in the classical level set method. In fact, this formulation was proved in [8] to lead to two important properties:

(i) Given $(c_{ij}) \in \mathbb{R}^4$, the problem (1) is convex in $u = (u_1, u_2) \in [0, 1]^2$, and therefore has a global minimum.

(ii) A region, which globally minimizes energy $E(u, c)$ on the space of binary functions, can be obtained by thresholding u_1 and u_2 at almost any value $\alpha \in [0, 1]$ ($\alpha = 0.5$ is the standard choice).

Thus, once the steady state is reached as stated by (i), the final image partition can be obtained according to (ii) by associating each voxel $x \in \Omega$ with a phase P_i, $i \in \{1..4\}$ in the following way:

$$\begin{cases} P_1 = \{x \mid u_1(x) \geq \alpha, u_2(x) \geq \alpha\} \\ P_2 = \{x \mid u_1(x) \geq \alpha, u_2(x) < \alpha\} \\ P_3 = \{x \mid u_1(x) < \alpha, u_2(x) \geq \alpha\} \\ P_4 = \{x \mid u_1(x) < \alpha, u_2(x) < \alpha\} \end{cases}$$

The main advantage of the method from [8] lies in its globally convex formulation while partioning the whole image domain preventing from overlaps and holes in the final segmentation.

According to (i), an alternate minimization scheme is proposed:

1. Set u_1 and u_2, then compute the weighted average MRI intensity c_{ij} for each phase:

$$c_{ij} = \frac{\int_\Omega \varphi_{ij}(u_1(x), u_2(x)) I_{\mathrm{MRI}}(x) dx}{\int_\Omega \varphi_{ij}(u_1(x), u_2(x)) dx} \tag{2}$$

2. Set c and u_2, then minimize:

$$\min_{u_1 \in [0,1]} \left\{ G_1(u_1) = \mu_1 \int_\Omega |\nabla u_1(x)| \, dx + \int_\Omega r_1(x) u_1(x) dx \right\} \tag{3}$$

where

$$r_1(x) = u_2(x) \left[\lambda_{11}(I_{\mathrm{MRI}}(x) - c_{11})^2 - \lambda_{01}(I_{\mathrm{MRI}}(x) - c_{01})^2\right]$$
$$+(1 - u_2(x)) \left[\lambda_{10}(I_{\mathrm{MRI}}(x) - c_{10})^2 - \lambda_{00}(I_{\mathrm{MRI}}(x) - c_{00})^2\right]$$

3. Set u_1 and u_2, compute the average MRI intensity as in 1.

4. Set c and u_1, then minimize:

$$\min_{u_2 \in [0,1]} \left\{ G_2(u_2) = \mu_2 \int_\Omega |\nabla u_2(x)| \, dx + \int_\Omega r_2(x) u_2(x) dx \right\} \tag{4}$$

where

$$r_2(x) = u_1(x) \left[\lambda_{11}(I_{\mathrm{MRI}}(x) - c_{11})^2 - \lambda_{10}(I_{\mathrm{MRI}}(x) - c_{10})^2\right]$$
$$+(1 - u_1(x)) \left[\lambda_{01}(I_{\mathrm{MRI}}(x) - c_{01})^2 - \lambda_{00}(I_{\mathrm{MRI}}(x) - c_{00})^2\right]$$

Our convergence criterion is based on stable $E(u, c)$, which means that the energy does not differ much from one iteration to another. In practice, convergence is reached in less than 1000 iterations. Steps 2 and 4 are implemented using the Chambolle's dual algorithm [8, 9]. Note that the weighted average MRI intensities c_{ij} are updated every iteration at steps 1 and 2, and not every n iterations at step 1 as suggested in [8], for a more precise optimization.

As in [5, 10], the constant regularization parameters μ_i, $i \in \{1, 2\}$ can be replaced by a contrast-dependent function defined as follows:

$$\mu_i(x) = \mu(x) = \frac{1}{1 + |\nabla G_\sigma * I_{\mathrm{MRI}}(x)|}$$

where a Gaussian kernel G_σ is used for robust gradient estimation. This map reduces the regularization where the edges are emphasized, which is characterized by a high contrast.

2.2. 3D multi-phase MR segmentation using PET information

The main challenge in our multimodal segmentation model is to use functional information provided by the PET image to guide the MR image segmentation while preserving anatomic boundaries. Thus, the resulting tumor volume is specific to the MRI data rather than being a compromise between the two modalities. The method from [5] addressed this issue in a two-phase framework to delineate lung tumors in CT. The main idea in [5] is to turn the scalar homogeneity weights in a spatial function $\lambda(x)$ of PET intensity to control the impact of each term of the energy functional $E(u, c)$. More precisely, while for high values of λ, the homogeneity prevails and the segmentation is mostly guided by the anatomic information, when λ takes low values, the smoothness prior is predominant. Moreover, λ was implemented in [5] as a sigmoid function so as to preserve the convexity property of the energy to minimize.

In our formulation, we follow the same underlying biological hypothesis, stating that the higher the PET intensity, the more likely the tumor presence, physiological tracer uptake excepted. This idea is also formulated by turning the scalar homogeneity weights λ_{ij} in spatial function $\lambda_{ij}(x)$ of PET intensity. Thus, the segmentation of the MR image is biased by PET intensity information, but remains consistent with the anatomic homogeneity and regularization constraints. Experimentally, simple positive increasing functions of PET intensity have shown to preserve the convexity of the energy to minimize. Compared to [5], the main difference in our implementation resides in the formulation of the spatial functions $\lambda : \mathbb{R} \longrightarrow [0, M]$ so as to reduce the number of parameters to set:

$$\lambda_{ij}(x) = \lambda(x) \; = \; M \, \frac{I_{\mathrm{PET}}(x) - mi}{ma - mi} \tag{5}$$

where $I_{PET}(x)$ is the PET intensity of voxel x, $ma = \max_{x \in \Omega} I_{\mathrm{PET}}(x)$, $mi = \min_{x \in \Omega} I_{\mathrm{PET}}(x)$ and M a positive hyperparameter.

The only hyperparameters to be set to solve the segmentation problem are now the M positive constant, describing the influence of PET image on the segmentation result, the standard deviation σ of the Gaussian kernel G_σ and the threshold α.

3. EXPERIMENTAL RESULTS

3.1. Material

The proposed method was evaluated using four patients suffering from atypical meningiomas. Before radiation therapy, these patients underwent a brain MRI followed by a whole body PET scan, which was acquired from 15 days to 6 months after the MR scan. The PET exam was performed with a PET/CT scanner (GE Discovery

LS, WEMS, Laukesha, WI, USA), using ^{18}F-choline as radiopharmaceutical and resulted into images with a $1.17 \times 1.17 \times 3.27mm^3$ sampling. After an initial injection of 3 to 3.5 MBq/Kg, the protocol included a dynamic aquisition (5 to 20 frames of 1 minute each), followed by a static whole-body acquisition, and a late acquisition centered on the brain was performed 60 minutes after injection. The Gd-enhanced T1-weighted MR were performed on different MRI machines and had different voxel sizes, as summarized in Table 1.

Tumor	Scanner	Voxel size (mm^3)
a	Siemens Aera 1.5T	$1.0 \times 1.0 \times 1.0$
b	Siemens Skyra 3T	$0.90 \times 0.90 \times 1$
c	Siemens Skyra 3T	$0.90 \times 0.90 \times 1$
d	Siemens Aera 1.5T	$1 \times 1 \times 0.99$
e	Siemens Skyra 3T	$0.51 \times 0.51 \times 1.2$

Table 1: Characteristics of MR images from the four patients (tumors b and c are from the same one).

Atypical meningiomas are very challenging to segment, owing to a high variability in terms of location, shape and signal intensity. Pathological radiotracer uptake in PET could help in differentiating tumor tissues from background surrounding structures with similar MRI intensity but PET images have a relatively high noise level. For all these reasons, the method was applied on a limited Volume Of Interest (VOI) defined manually.

3.2. Hyperparameter setting

The PET images from the late acquisition were aligned to the T1-Gd images via the Mipav software[1] using normalized mutual information-based registration. The threshold parameter for u_1 and u_2 was set to $\alpha = 0.5$. A $3 \times 3 \times 3$ Gaussian kernel with standard deviation $\sigma = 1$ voxel was used for contrast estimate. Values for M ranging from 10 to 500 with a step of 10 were tested. The phase corresponding to the tumor was initialized by thresholding at 40% of the maximum PET intensity value within the VOI, while the remaining volume was initialized using a three class k-means algorithm applied to the MR. After the final thresholding, the phase with the highest PET mean intensity was assigned to the tumor.

3.3. Results

The segmentations were evaluated against a manual MR tumor delineation performed by a medical expert who had a prior knowledge of the PET exam. The computational time for the tumor segmentation was about 3-4 minutes on MATLAB2012b on a Linux desktop computer with Intel Core Xeon(R) CPU 3.7 GHz,15 GB RAM using VOIs containing 50000 voxels on average. The Dice index obtained by testing with different values for M in a model incorporating PET intensity information or no prior information (*i.e* $\lambda(x) = M$) showed that the typical ranges of M leading to relevant results are different depending on whether PET information is taken into account or not, and, in each case, are prone to inter-patient variability. As illustrated in Figure 1, one of the three values $M = 50$, 100 or 150 always gave a relevant qualitative result.

As shown in Figure 2, though introducing PET information may result into altering the convexity of $E(u, c)$ (which holds when no prior information is used), the algorithm still manages to reach a global minimum and provides an appropriate segmentation.

Moreover, the results obtained by testing the three values of M, with or without PET information, showed that using PET intensity to

[1] mipav.cit.nih.gov

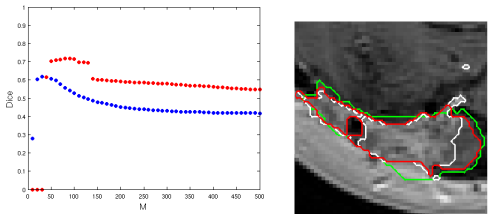

(a) **(b)**

Fig. 1: Segmentation results for Tumor a: (a) Plot of Dice index as a function of M with no prior information (in blue) or with PET intensity information (in red). (b) Manual (in green) *vs.* automated segmentations obtained with no prior information with $M = 50$ (in white) and with PET intensity information with $M = 100$ (in red).

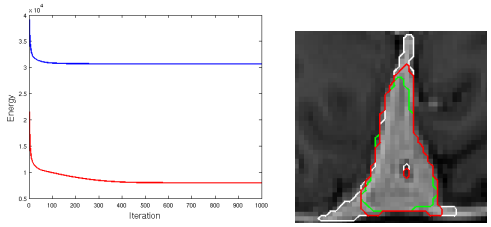

(a) **(b)**

Fig. 2: Segmentation results for Tumor b: (a) Plot of the energy $E(u, c)$ during the iterative optimization process with no prior information (in blue) or with PET intensity information (in red) with the same value $M = 50$. (b) Manual (in green) *vs.* automated segmentations obtained with no prior information (in white) and with PET intensity information (in red) with the same value $M = 50$.

guide the segmentation led to a more accurate tumor segmentation of the MRI than when no PET information is used, and can prevent from including non-tumor neighboring structures with similar MRI intensities (Figure 3). This result is quantitatively confirmed by the Dice indices, measuring the overlap between automatic and manual segmentations, and the sensitivity and specificity indices, respectively measuring the rate of voxels correctly assigned to the tumor and non-tumor volume (Table 2). Multiple experts study would be necessary to strengthen this conclusion, since manual segmentation of atypical meningiomas is a tedious task that can suffer from a great inter-operator variability. The worst qualitative and quantitative result was observed for the heterogeneous Tumor d as shown in Figure 3b, which suffers from postoperative tissue reorganization.

Tumor	a	b	c	d	e
Dice SegMRI	0.59	0.58	0.55	0.43	0.61
Dice SegPET-MRI	0.71	0.76	0.72	0.44	0.65
Sensitivity SegPET-MRI	0.63	0.96	0.88	0.31	0.55
Specificity SegPET-MRI	0.99	0.99	1.00	0.99	0.99

Table 2: Quantitative comparison between manual and the best automatic segmentation result obtained using $M = 50, 100, 150$ with (SegPET-MRI) or without (Seg-MRI) PET information.

Dealing with atypical meningiomas, a four-phase model turned out to be generally more efficient to distinguish between the tumor and surrounding tissues with similar MRI intensities than a two-phase formulation, as illustrated in Figures 4a and 4c. However, a four-phase formulation can provide results similar to those delivered by a two-phase model, as illustrated in Figure 4b.

As shown in Figure 5, the drawing of the VOI influences the results when guiding segmentation with PET intensity. Indeed, the segmentation is sensitive to the noise in the PET image.

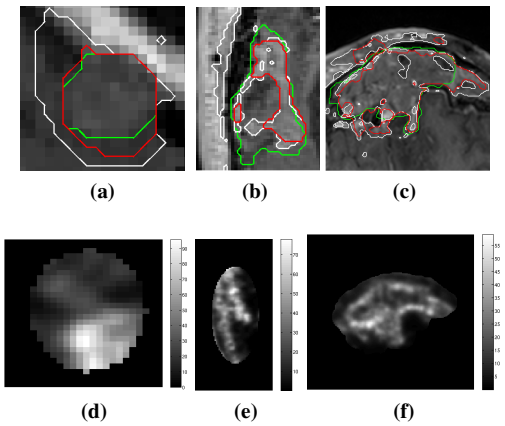

Fig. 3: Comparison between manual (in green) and automatic segmentations of the tumor guided by PET intensity information (in red) or with no prior information (in white) of Tumors c (a), d (b) and e (c). λ map used to guide the segmentation with PET information for Tumors c (d), d (e) and e (f).

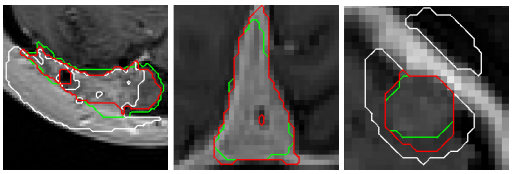

Fig. 4: Influence of the number of phases: visual comparison between manual (in green) *vs.* automatic segmentations of the tumor guided by PET intensity information using a two-phase (in white) and four-phase (in red) model for Tumors a (a), b (b) and c (c).

4. DISCUSSION AND CONCLUSION

The goal of this paper was to extend a 3D PET-guided two-phase globally convex variational segmentation method to a 3D four-phase framework to address the variability of the MR signal in the surrounding of the tumor. Guiding a multi-phase segmentation by functional information was proven to be a solution to distinguish between tumor tissues and structures with similar mean intensities. Moreover, guiding the anatomical segmentation by functional information made the result closer to the manual delineation. However, this model has currently two limitations. First, it was used on manually drawn VOIs influencing the final segmentation result. Secondly, the piecewise constant formulation of the segmentation model may be unsuited for heterogeneous tumors. In our future work, these two issues will be addressed by performing an automated detection of the tumor VOI, and using other image approximation models. The method will also be applied to a larger data set, including cerebral lesions such as glioma, and tested with scans produced from an hybrid PET-MRI device so that PET and MR data do not need to be registered. The results can then be the input of a clinical study to determine, from retrospective studies, how the tumor volume estimated from each modality should be used to define treatment plan in a radiation therapy.

5. ACKNOWLEDGMENTS

This work is supported by the "Lidex-PIM" project funded by the IDEX Paris-Saclay, ANR-11-IDEX-0003-02. Thanks to Dr. J.L Alberini from Hôpital René Huguenin (Saint-Cloud, 92, France) for providing images.

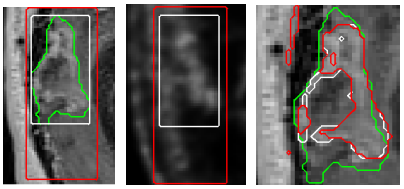

Fig. 5: Influence of the VOI: Manual segmentation of the MR tumor (in green) for two VOIs (in white and red) on the MR image (a). (b) Superimposing of the two VOIs (in white and red) on the PET image (b). (c) Visual comparison between manual (in green) *vs.* automatic segmentations of the tumor guided by PET intensity information in a four-phase model for the two VOIs.

6. REFERENCES

[1] U. Bagci, J.K. Udupa, N. Mendhiratta, B. Foster, Z. Xu, J. Yao, X. Chen, and D.J Mollura, "Joint segmentation of anatomical and functional images: Applications in quantification of lesions from PET, PET-CT and MRI-PET-CT images," *Medical Image Analysis*, vol. 17, pp. 929–945, 2013.

[2] Z. Xu, U. Bagci, J.K. Udupa, and D.J Mollura, "Fuzzy Connectedness Image Co-segmentation for Hybrid PET/MRI and PET/CT Scans," in *Computational Methods for Molecular Imaging*, pp. 15–24. Springer, 2015.

[3] Q. Song, B. Junjie, D. Han, S. Bhatia, W. Sun, W. Rockey, J.E. Bayouth, J.M. Buatt, and X. Wu, "Optimal Co-Segmentation of Tumor in PET-CT Images With Context Information," *IEEE Transactions on Medical Imaging*, vol. 32(9), pp. 1685–1697, 2013.

[4] U. Bagci, G. Kramer-Marek, and D.J. Mollura, "Automated computer quantification of breast cancer in small-animal models using PET-guided MR image co-segmentation," *EJNMMI Research*, vol. 3(1), pp. 1–13, 2013.

[5] J. Wojak, E.D Angelini, and I. Bloch, "Joint variational segmentation of CT-PET data for tumoral lesions," in *IEEE International Symposium on Biomedical Imaging: From Nano to Macro*, 2010, pp. 217–220.

[6] T.F. Chan, S. Esedoglu, and M. Nikolova, "Algorithms for finding global minimizers of image segmentation and denoising models," *SIAM Journal on Applied Mathematics*, vol. 66(5), pp. 1632–1648, 2006.

[7] T.F. Chan and L. Vese, "Active contours without edges," *IEEE Transactions on Image Processing*, vol. 10(2), pp. 266–277, 2001.

[8] J.C Moreno, V.B.S Prasath, H. Proença, and K. Palaniappan, "Fast and globally convex multiphase active contours for brain MRI segmentation," *Computer Vision and Image Understanding*, vol. 125, pp. 237–250, 2014.

[9] A. Chambolle, "An algorithm for total variation minimization and applications," *Journal of Mathematical Imaging and Vision*, vol. 20(1-2), pp. 89–97, 2004.

[10] X. Bresson, S. Esedoglu, P. Vandergheynst, J.P. Thirian S., and Osher, "Fast global minimization of the active contour/snake model," *Journal of Mathematical Imaging and Vision*, vol. 28(2), pp. 151–167, 2007.